RSC Advances

ROYAL SOCIETY OF CHEMISTRY

www.rsc.org/advances

Graphic Abstract

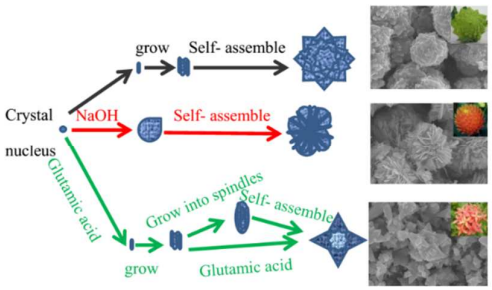

Three-dimensional (3D) ZnO materials with different morphologies were fabricated and the mechanism for the formation of these ZnO nanoaggregates proposed.

RSC Advances

RSCPublishing

ARTICLE

Preparation of diverse flower-like ZnO nanoaggregates for dye-sensitized solar cells

Cite this: *RSC Advances, xxxx,xxxx*

Liping Lin,[a,b] Xiao Peng[a] and Si Chen[a] , Bao Zhang[a*], Yaqing Feng[a,b**]

Received 00th xxxxxxx 2015,
Accepted 00th xxxxxxxx 2015

DOI: 10.1039/x0xx00000x

www.rsc.org/advances

Three-dimensional (3D) ZnO nanoaggregates with different morphologies and sizes were fabricated by the hydrothermal method, including cauliflower-like microspheres with average diameter of 1–2 μm, nano-sheets aggregated safflower-like microspheres with 3–4 μm and ixora-like nano-structures with 500–600 nm. We found that their morphology formation was dependent on the concentration of OH^- and construction agent (glutamic acid) during the synthesis process, based on which we proposed the mechanism for the formation of ZnO nanoaggregates. The studies showed that, the photo to current conversion efficiencies (PCEs) of the dye-sensitized solar cells (DSSCs) in which the photoanodes were fabricated using the prepared 3D ZnO nanoaggregates were all higher than those obtained employing the ZnO nanoparticles (NPs). In particular, the PCE of the DSSC based on cauliflower-like ZnO photoanode (4.52%) was about 21% higher than that fabricated with ZnO NP-based photoanode. This can be attributed to the higher specific surface area of the cauliflower-like ZnO photoanode leading to greater amount of dye adsorption, more suitable size for light scattering and better inner connection for the transportation of electrons. Moreover, when these 3D ZnO nanoaggregates were used as the scattering layers in the P25-based photoanode in DSSCs, higher PCE of up to 6.74% was achieved, compared to 5.37% obtained for the DSSC without scattering layer.

1. Introduction

Dye-sensitized solar cells (DSSCs) have attracted much attention, due to their low cost and simple workmanship.[1] DSSCs consist of counter electrode, electrolyte and photo-anode absorbed by organic dyes.[2] To date, most researchers have chosen TiO_2 as the DSSC photoanode[3], and the highest photo to current conversion efficiency (*PCE*) of more than 11% was achieved with N719 as the sensitizer.[4] The efficiency even exceeded 13% by using porphyrin sensitized TiO_2 photoanode.[5] However when it comes to photoanode semiconductor, ZnO is still regarded as a promising alternative to TiO_2,[6] because of its better electron mobility, significantly longer electron lifetime[7] and easier fabrication of different morphologies of nanostructures.[8]

Similar to TiO_2, ZnO has a wide band gap (3.37eV) and large excitation binding energy (60meV).[9] Up to now, ZnO nanomaterial with various morphologies have been synthesized,[10] such as 0-dimensional (0D) nanoparticles[11], 1D nanowires, nanofibers, nanotubes, nanobelts, etc[12-15], 2D nanosheets[16], 3D microspheres[17-18] and so on. More and more researchers have devoted to synthesizing 3D and hierarchical ZnO as the semiconductor of the DSSCs[19-20]. For example, Zhang and co-workers have synthesized 3D aggregation of ZnO nanocrystallites for the polydisperse film of DSSC, which achieved a *PCE* of up to 5.4%.[21] The highest efficiency based on ZnO photoanode was 7.5% reported by Memarian[22] and co-workers. They introduced a hierarchical ZnO layer which was shown to be able to improve the light absorption, enhance the light scattering and inhibit the back electron transfer. Similarly, Lu[23] has prepared multi-dimensional ZnO architecture as DSSC photoanode (including 2D ZnO nanosheets and 3D ZnO nanoaggregates), and with 0D ZnO nanocrystal as the compact layer, the DSSC led to an impressive *PCE* of 7.35%.

At the same time, the improvement of the light harvested by the photoanode is also a vital factor in influencing the *PCE*, which has attracted much attention. In addition to designing the more efficient dye molecules, the enhancement of light scattering by introducing a scattering layer in a photoanode is also an effective way to improve light harvest. Weiwei Sun and co-workers synthesized layer-by-layer self-assembled TiO_2 hierarchical nanosheets (TiO_2 LHNs) with exposed {001} facets, which exhibit favourable light scattering effect. As a result the photoelectric conversion efficiency of 7.70 % has been achieved for the DSSCs using TiO_2 LHNs as the bifunctional layer indicating 21% improvement compared to the pure P25 (6.37%) as photoanode.[24] Mahmood fabricated a double light-scattering-layer in a boron-doped ZnO film-based DSSC which achieved a *PCE* of 7.2%.[25]

Even though up to 7.5% *PCE* was achieved when ZnO is employed as the semi-conductor material of the photoanode, there are still many issues to be addressed. For example, it is known that 1D ZnO has the best electron mobility, but its specific surface area (*SSA*) is too small to adsorb enough dye. On the other hand, 3D ZnO has larger *SSA*, but the electron mobility is reduced. In order to obtain a ZnO material with large *SSA* while maintain its high electron mobility, we prepared 3D ZnO nanoaggregrates (nanoflowers) with different

morphologies. The nanoaggregrates having been fabricated are all featured with wurtzite structure and the constituent units are all single crystal. These ZnO nanostructures can make sure good electron mobility and possess large *SSA* simultaneously. The morphologies of prepared ZnO nanoaggregrates were controlled by changing the concentration of OH^- and construction agent. By using N719 as the sensitizer, a *PCE* of up to 4.52% was achieved for the DSSC fabricated with these ZnO nanoaggregates as photoanode material, whereas for the ZnO NP-based DSSC under our experimental conditions, the conversion efficiency of only 3.73% was realized. Furthermore, when these ZnO nanoaggregates were employed as light scattering layers for P25-based DSSCs, the *PCE* was significantly improved from 5.37% (for a P25-based DSSC without any light scattering layer) to 6.74%, which means a 25.5% enhancement.

2. Experimental

Main materials

Zinc acetate dihydrate ($ZnAc_2$•2H2O), L-glutamic, NaOH, ethyl cellulose (EC), absolute ethanol and acetonitrile were obtained from Guangfu Chemical Reagent Co., China. Other chemicals such as 1,2-dimethyl-3-propylimidazoliumiodide (DMPII), terpineol (Aladdin), valeronitrile (J&K), LiI, I_2, 4-tert-butylpyridine (4-TBP), GuSCN (Dalian HeptaChroma SolarTech Co., Ltd.,), potassium persulfate (KPS) (Jiangtian Chemical Reagent Co., China), P25 (Degussa AG, Germany), and N719 (Solaronix, Switzerland.) were all purchased and used without further purification. Fluorine-doped tin oxide substrate (FTO) (Nippon, Japan, 15Ω/square) was ultrasonically cleaned with distilled water and ethanol respectively.

Preparation of ZnO nanoaggregates

The ZnO nanoaggregates were prepared as following: 0.5 mmol of glutamic acid were dissolved in 10 mL aqueous solution of $ZnAc_2$•$2H_2O$ (0.1 M), and 10 mL aqueous solution of NaOH (0.4 M) was poured into the aforementioned solution under stirring. The as-prepared suspension was then transferred to a 30 mL Teflon autoclave and maintained at 150℃ for 10 h. After cooling down to ambient temperature, the white precipitate was centrifuged, washed with distilled water and absolute ethanol for three times respectively, and dried at 70℃. In this way, 3D ZnO nanoaggregate was obtained, which looks like a cauliflower (as shown in the later scanning electron microscopy image) and is denoted as sample **1**. Sample **2** （safflower-like） was prepared with the same method, except that the concentration of NaOH was changed to 0.8mM. Sample **3** （ixora-like） was also prepared with the same method, except that the amount of glutamic acid was changed to 1 mmol.

The ZnO NP was prepared using a method described by Agez and co-workers.[11] $ZnAc_2$•$2H_2O$ (4.4 g) was dissolved in 100 mL methanol to obtain a 0.2 M solution which was stirred at room temperature overnight. Then aqueous NaOH solution (3 M) was added dropwise to the aforementioned solution under vigorous stirring until that the final pH value was adjusted to 12. A white suspension was obtained and kept stirring for 12 h at room temperature. The suspension was then washed with ethanol and centrifuged three times. The obtained ZnO NP was thus stored as a suspension in ethanol. ZnO NP suspension (1 g) was dried under 70℃ to examine the solid mass fraction, which was repeated for three times. The average value of the solid mass fraction was then determined.

Preparation of ZnO films and fabrication of DSSCs

To prepare the paste for ZnO films, 0.8 g ZnO nanoaggregates, 0.2 g P25, 0.5 g ethyl cellulose (EC), 3.5 g terpineol, and 30 g ethanol were mixed and grinded by ball grinder for 3 h. The mixture was then concentrated with rotary evaporator and the residue was grinded with mortar to achieve the homogeneous paste. The paste of NP was prepared with the same method, except that the NP was added according to the mass fraction in the suspension.

FTO was ultrasonically cleaned with water and ethanol separately and treated with 50 mM $TiCl_4$ at 70℃ for 30 min. The above-prepared pastes were then spread onto FTO by doctor-blade method to obtain the films, which were annealed at 500℃ for 1 h and treated with 50 mM $TiCl_4$ at 70℃ for 0.5 h. The resultant films were calcinated at 500℃ for another 30 min. The final films were composed of 15~18 μm ZnO layers and 4~6 μm TiO_2 layers and the SEM images of the profiles of these films are given in Fig. S1. The area of the films are 0.159 cm^2, which could be controlled by the doctor-blade method. The films were then immersed into an ethanol solution of N719 (3×10^{-4} M) for 2 h after cooling down, followed by being cleaned with ethanol and dried at room temperature. The photoanode was assembled with Pt counter electrode and electrolyte to form a sandwich-type cell. The injected electrolyte consisted of 0.6 M DMPII, 0.03 M I_2, 0.5 M 4-TBP and 0.1 M GuSCN in a mixed solvent of acetonitrile and valeronitrile in a volume ratio of 85/15.

Characterization

The structure properties of the ZnO nanoaggregates were characterized by the powder X-ray diffraction (XRD, Bruker D8-focus diffractometer).The micro-morphology of ZnO crystals were characterized by scanning electron microcopy (SEM). The *SSA* of ZnO powder was analyzed by Brunauer-Emmet-Teller (BET) measurement. The *I-V* curves were measured using a solar simulator (solar AAA simulator, Oriel China), under AM 1.5, which was adjusted using a calibrated Si solar cell (National Institute of Metrology, China), and recorded with a computer-controlled digital source meter (Kethily 2400). To determine the amount of dye adsorption, the sensitized photoanode was immersed into a 0.1 M solution of NaOH in water and ethanol (volume ratio of 1:1), and the absorption spectrum of the desorbed dye solution was measured by a UV-vis spectrophotometer. A 300 W xenon lamp (Newport, USA) was used to give incident light ranging from 400 to 700nm for the incident photo-to-electron conversion efficiency (IPCE) measurements. Electrochemical impedance spectrum (EIS) measurement and open-circuit voltage decay (OCVD) characteristics of the devices was carried out by using electrochemical workstation (CHI660 Chenhua, China) to determine the electron transport characteristics, and the bias voltage was set as the open current voltage (V_{OC}) of DSSC under an AM 1.5 G solar illumination of 100 mW/cm^2.

3. Results and discussion

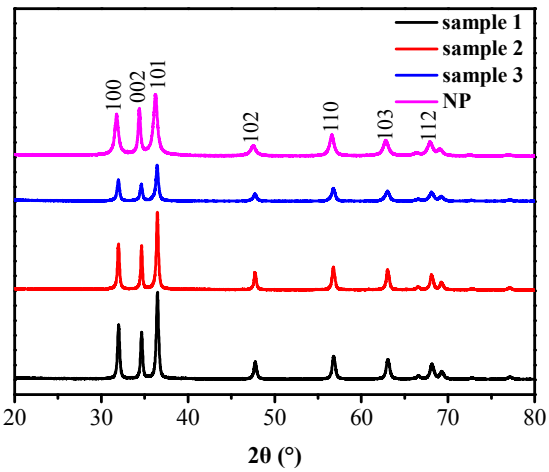

Fig. 1 XRD patterns of the ZnO nanoaggregates (sample **1**, sample **2**, sample **3**) and NP.

Figure 1 shows the XRD patterns of sample **1** (cauliflower), sample **2** (safflower), sample **3** (ixora) and NP. All the diffraction peaks observed are well indexed to wurtzite hexagonal structured ZnO (JCPDS card No. 36-1451). No other peaks were detected, which means no residual reactants or intermediates were present. It is known that the sharper diffraction peaks could imply the higher crystallinity. Therefore, based on the XRD patterns, the crystallinity of these ZnO aggregates could be qualitatively compared and the order can be estimated as following: sample **1**> sample **2**> NP> sample **3**.

The SEM images show the morphologies of the ZnO nanoaggregates and NP. Sample **1** is composed of cauliflower-like microspheres with average diameter between 1–2μm (Fig. 2a). Sample **2** is composed of safflower-like microspheres between 3–4 μm (Fig. 2b), which is aggregated by nanosheets. Sample **3** is composed of ixora-like nano-flower crystals between 500–600 nm (Fig. 2c). It is also clear from the SEM image (Fig. 2d) that the average diameter of NP is about 30nm.

Figure 3 shows the TEM images of sample **1** (Fig. 3a), sample **2** (Fig. 3b), sample **3** (Fig. 3c), and NP (Fig. 3d). The images demonstrate that, sample **1** (cauliflower) and sample **3** (ixora) have better inner connection than sample **2** (safflower), which is assembled by nanosheets. Figure 3d can also illustrate that the ZnO NPs are dispersed homogeneously. The lattice fringe images show that the d-spacing values of the samples we prepared are around 0.264 nm, which is similar to the (001) plane of ZnO, and that of NP is 0.246 nm, which is similar to the (101) plane of ZnO. Besides the crystal size of the prepared samples are all larger than that of NP, which is corresponding to the XRD pattern. Moreover the lattice fringe arraying in the same direction in a wide range may indicate the prepared samples are constructed by single-crystals. The selected area electron diffraction (SAED) images can further demonstrate that, the ZnO nano-materials are all constructed by single-crystals.

Based on the above results, we proposed the mechanism for the formation of ZnO nanoaggregates with different morphologies. As is shown in Figure 4, the crystal nucleus of ZnO grows into short rods when the ratio of $ZnAc_2$: NaOH equals 1:4. The short rods self-assemble into the cauliflower-like microspheres when $ZnAc_2$: glutamic acid equals 2:1, but grow into spindles and then self-assemble into ixora-like nanostructure when the ratio of $ZnAc_2$: glutamic acid is 1:1. On

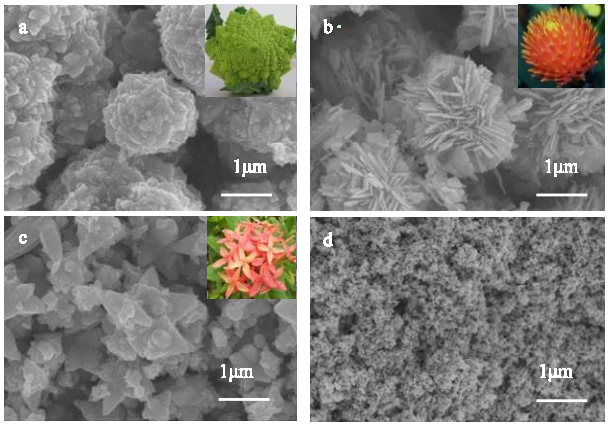

Fig. 2 SEM images of the nanoaggregates (a, sample **1** (cauliflower); b, sample **2** (safflower); c, sample **3** (ixora)) and NP (d).

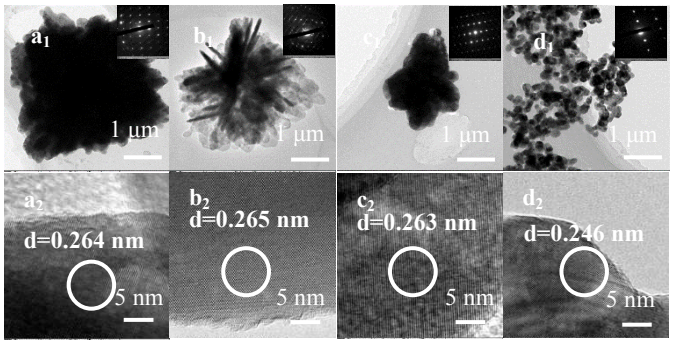

Fig. 3 TEM and SEAD images of the nanoaggregates (a, sample **1**; b, sample **2**; c, sample **3**) and NP (d).

the other hand, the nucleus grows into nanosheets when the ratio of $ZnAc_2$: like micro-spheres subsequently. It is known that, ZnO is easy to form rod-like structure in basic solution when no construction agents exist, because the surface energy of (001) plane is high.[26] In order to demonstrate this, the experiment without glutamic acid was also designed and it was found that ZnO with nano-rods structure (Fig. S2) was obtained. The esperiment was taken as afore-mentioned, except that no glutamic acid was add into the $ZnAc_2$ solution. It was reported that the presence of histidine minimizes the tendency of ZnO to form larger, elongated crystals.[27] It is believed that the presence of glutamic acid will affect the growth of ZnO crystals in the same way. That is to say, when OH^- plays the leading role, ZnO will grow to form larger and elongated crystals, but with the presence of glutamic acid, nanosheets were formed, leading to safflower-like microspheres (sample **2**). On the contrary, when glutamic acid plays the main role, rod-like ZnO crystals will stop growing further and begin to assemble to larger units. The larger units then self-assemble and grow into cauliflower-like microspheres (sample **1**), when the concentration of glutamic acid is 0.5 M. When the concentration of glutamic acid increases to 1 M, the larger ZnO crystal units continued growing into spindles, which self-assemble and grow into ixora-like nano-structure (sample **3**). To further demonstrate our proposal, the "time-dependent experiment" was performed. The SEM images of ZnO nanomaterials were obtained when the hydrothermal temperature was kept at 150℃ for 0.5 h, 1 h,

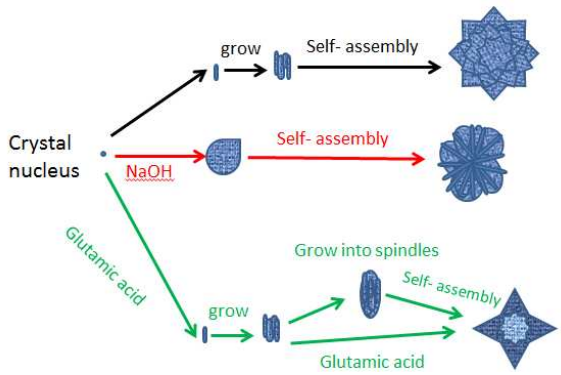

Fig. 4 Schematic illustration of the formation of nanoaggregates.

2 h, 4 h, 6 h and 8 h. The SEM images of the "time-dependent experiment" can be found in supplementary information (Fig. S3, Fig. S4, Fig. S5). Figure S3 shows the SEM images of the formation of sample **1**. At the beginning of the experiment, the units of the microspheres are slight. As time passes by, the units grow up and the connection of them becomes better and the cauliflower-like microspheres were formed. Figure S4 gives the SEM images of the formation of sample **2**. At first, the nanosheets are slight and assemble in disorder. Gradually, the nanosheets grow up and form the safflower-like microspheres. Figure S5 shows the SEM images of the formation of sample **3**. The units grow up similar to sample **1**. At the same time, there are some single units in Fig. S5a, and the single units become less as time passes by, which proves that the units self-assemble to form the ixora-like nano-structure. These results further demonstrate the mechanism we proposed.

Next, the N719-sensitized solar cells were fabricated with prepared ZnO aggregates with different morphologies as photoanodes. Photovoltaic properties of these cells were examined with an active area of 0.159 cm^2 using sunlight simulator, and the step of scanning was 10 mV.

Figure 5 shows the photocurrent density (*I*)-voltage (*V*) curves of DSSCs based on four kinds of ZnO nanoaggregates films (sample **1**, sample **2**, sample **3**, and NP) respectively. The corresponding photovoltaic properties of these cells are collected in Table 1. Figure 6 shows the UV-vis spectra of dye solution desorbed from DSSCs based on sample 1, 2, 3 and NP. The amount of dye adsorption can be calculated according to the peak value around 500 nm. The corresponding data of amount of dye absorption are listed in Table 1. To better understand the correlation between the cell performance and the material properties, the *SSA* data are also listed in Table 1.

The overall efficiencies of the devices display a trend of decrease from sample **1** (4.52%), sample **3** (4.23%), sample **2** (4.13%), to NP (3.73%), as is shown in Table 1. The highest the J_{SC} values of sample **3**, sample **2** and NP-based cells are all lower than that of sample **1**. Based on the amount of dye adsorption shown in Table 1, the lower J_{SC} values obtained for sample **3** and conversion efficiency was achieved for sample **1** (cauliflower)-based solar cell, which exhibits a *PCE* of 4.52% with J_{SC} = 7.86 mA/cm^{-2}, V_{OC} = 794 mV, and *FF* = 72.32%. It is noticeable that sample **2**-based cells can be attributed to the lower dye loading concentration on the surface of ZnO films, which is determined by the *SSA*.

It is believed that with greater *SSA*, the ZnO of the photoanode can provide more effective adsorption sites for dye, which will certainly increase the dye loading amount and the Jsc values. Therefore, the greatest *SSA* and dye loading amount

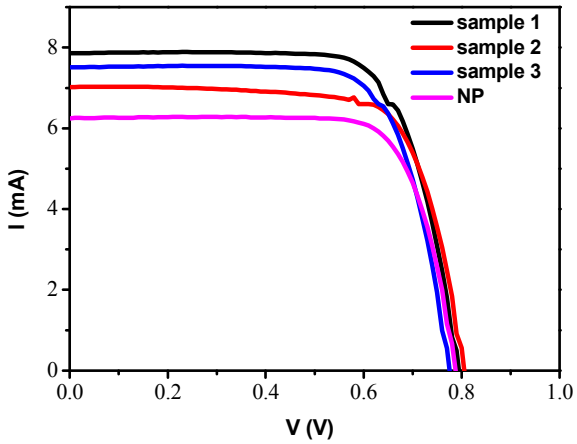

Fig. 5 Photocurrent- voltage curves of DSSCs based on photoelectrode films sample **1**, **2**, **3**, and NP.

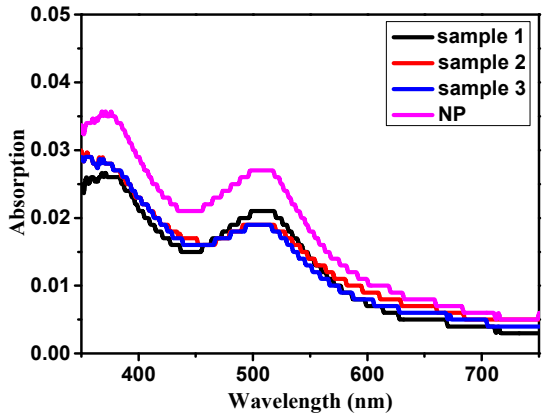

Fig. 6 The UV-vis spectra of dye solution desorbed from DSSCs based on photoelectrodes sample **1**, **2**, **3** and NP.

Table 1 *SSA* data, and photovoltaic properties of the solar cells measured under AM1.5G filtered 100 mW cm^2 illuminations

Sample	J_{SC}/mA	V_{OC}/mV	*FF*/%	η/%	Amount of dye adsorption/10^{-7}mol	*SSA*/m^2/g
sample **1**	7.86	794	72.32	4.52	3.42	27.8
sample **2**	7.02	805	73.06	4.13	3.11	24.1
sample **3**	7.51	755	72.68	4.23	3.11	24.9
NP	6.24	787	75.86	3.73	4.35	40.2

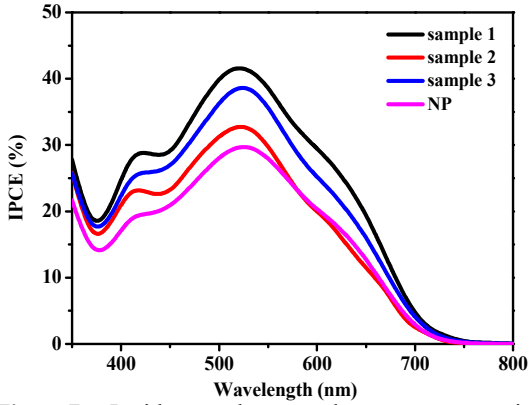

Fig. 7 Incident photo-to-electron conversion efficiencies as a function of wavelength for devices composed of sample **1**, **2**, **3** and NP.

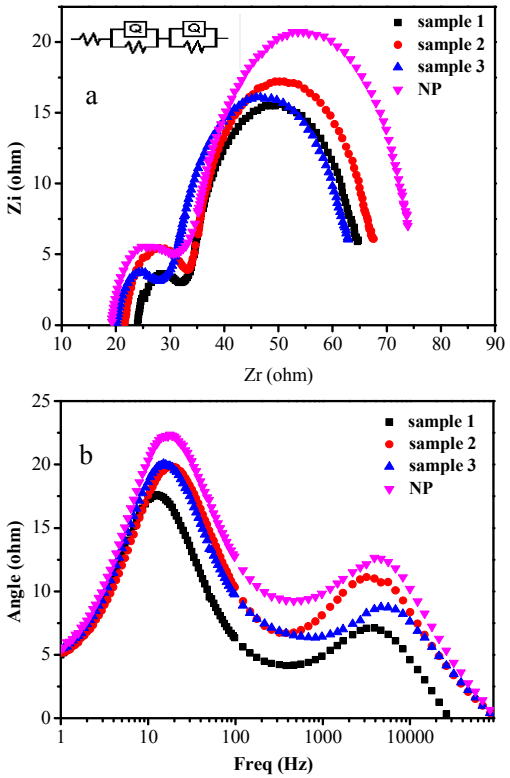

Fig. 8 Nyquist (a) and Bode (b) plots of DSSCs based on different ZnO photo-anodes(sample **1**, **2**, **3**, and NP).

for sample **1** among three newly developed ZnO nanoaggregates result in the highest J_{SC} value and eventually the *PCE* value.

Interestingly, although NP has the largest *SSA* among all the ZnO materials and NP ZnO photoanode exhibits the greatest dye loading amount as shown in Table 1, all the DSSCs based on the newly prepared ZnO nanoaggregates achieved higher *PCE* than that based on NP. This should be attributed to better interconnection between the units of nanoaggregates. All the materials we fabricated are aggregated by nano-units, which self-aggregated into the resultant nanostructures and connected perfectly as shown in the TEM images (Fig. 3a, 3b and 3c). On the other hand, the interconnection between the nanoparticles is poor (Fig. 3d). As a result, the electrons are easier to transport in DSSCs based on newly prepared ZnO nanoaggregates, which eventually leads to greater J_{SC} and *PCE* values than NP ZnO-based DSSCs.

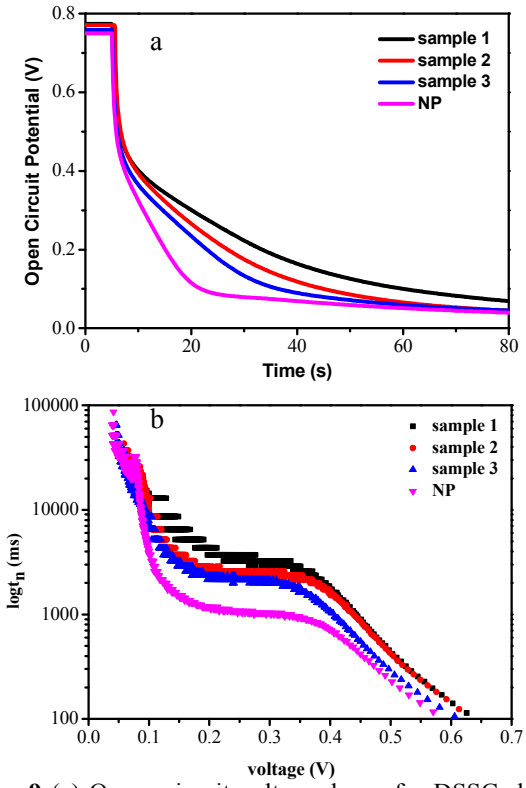

Fig. 9 (a) Open- circuit voltage decay for DSSCs based on sample **1**, **2**, **3** and NP. (b) Electron lifetime (in log-linear representation) as a function of open-circuit voltage for DSSCs based on sample **1**, **2**, **3** and NP.

Furthermore, the sample **1** has higher degree of crystallinity than other newly prepared ZnO nanoaggregates as discussed in the XRD patterns. Therefore, the electrons are also easier to transport in sample **1**-based DSSC, which results in the highest *PCE* values among all the fabricated cells.

Figure 7 shows the Incident photo-to-electron conversion efficiency (IPCE) spectra of the DSSCs, which varied in the range from 350 nm to 800 nm. The IPCE of the DSSC based on sample 1 is the highest in all the ranges, and the others are also in accord with the order of the J_{SC} and *PCE* values obtained in Table 1. These results further demonstrate the influence of the properties (*SSA* and the particle interconnection in the photoanode) of the ZnO nanoaggregates on the cell performance.

Figure 8 exhibits the EIS spectra of the DSSCs. Figure 8a is the Nyquist plots, which all have two semi-circles. Figure 8b shows the Bode plots the DSSCs correspondingly. The corresponding fitting results determined from EIS analysis are collected in Table 2. The internal impedances were determined by fitting the experimental data with an equivalent circuit (inset of Fig. 8). As is known that the semicircle in the higher frequency range of 100 Hz to 1 MHz refers to the charge-transfer resistance at the conducting layer/photoanode and counter electrode/electrolyte (R_1, the first semicircle in the Nyquist plot), and R_2 is ascribed to the charge transfer resistance at the photoanode/electrolyte interface (the second semicircle in the Nyquist plot). R_S is the transport resistance of the electrons in the photo-anode and the FTO/ZnO contact,

whose semicircle cannot be seen actually.[27] From the Nyquist plot it can be seen that the second semicircles of the DSSCs based on nanoaggregates are all smaller than that of the DSSC based on NP, and the DSSC based on sample **1** shows the smallest semicircle. This is corresponding to the R_2 value listed in Table 2. That is to say, the resistance of electron transport is lowest in the DSSC based on sample **1**.

Table 2 Electrochemical parameters determined from EIS analysis

Sample	R_S/ohm	R_1/ohm	R_2/ohm	f/Hz	τ/ms
sample **1**	28.83	18.5	40.27	14.7	10.83
sample **2**	27.72	17.79	48.63	21.5	7.40
sample **3**	26.49	15.99	45.59	21.5	7.40
NP	21.77	18.99	53.69	26.1	6.10

In the Bode phase plots (Fig. 8b), the frequency peak is indicative of the charge-transport process of injected electrons in ZnO. There are two peaks in the Bode plots, and the frequency of the first peak decides the electron lifetime. The data of the frequencies and the calculated electron lifetime are given in table 2. The results suggest that the DSSCs based on nanoaggregates all have longer electron lifetime than that based on NP, and that based on sample **1** has the longest electron lifetime of 10.83ms. The results from the Nyquist and Bode plots further explained the orgin of the greatest *Jsc* and *PCE* values obtained for the sample **1**-based DCCS.

The OCVD (the open-circuit voltage decay) characteristics of the devices were measured to further investigate the electron lifetime. Figure 9a illustrates the voltage decay curves respectively. Figure 9b is the curves calculated by the following equation.

$$\tau_n=(\kappa_B T)/e\ (dV_{oc}/dt)^{-1}$$

The value of the curve at high voltage (>0.6 V) mainly reflects the electron lifetime in the photoanode under working conditions.[28] The results are consistent with the EIS analysis, which indicates that the DSSC based on sample **1** has the longest electron lifetime laeding to the highest *PCE* value.

4. The effect of ZnO nano-structures as photo-scattering layers

To further demonstrate the utilities of our newly developed ZnO nanoaggregates, DSSCs based on P25 photoanodes with those ZnO nanoaggregates as photo-scattering layers were fabricated. Sample **1** was taken as an example as the photo-scattering layers in the P25-based DSSC, and as a comparison, P25-based DSSCs with NP as the scattering layer and without scattering layers were also made. All the devices are fabricated as mentioned beforehand, except that a layer of ZnO paste was then spread onto the surface of the P25 films as the photo-scattering layer after the P25 layer was dried at 70℃. Figure 10 shows the IV curves of these DSSC devices and the corresponding photoelectrical properties are collected in Table 3. It is obvious that the DSSC with sample **1** as the scattering layer has the highest J_{SC} and achieve the highest *PEC* of 6.74%, which is 25.5% higher than that obtained by the DSSC based on P25 without any photo-scattering layer. Interesting even when NP was used as the photo-scattering layer, a *PEC* of 6.11% was realized, which is also higher than that obtained by the DSSC without any scattering layers. It is believed that although NP has larger *SSA* for the adsorption of dye, sample **1** has more appropriate size of 700–800 nm for light scattering which leads to higher *PCE*. The results demonstrate that the ZnO nanoaggregates we prepared are also suitable for use as the scattering layers.

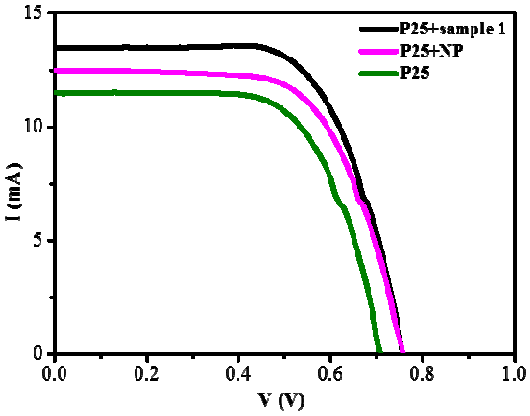

Fig. 10 Photocurrent-voltage curves of DSSCs based on P25 with and without photo-scattering layers.

Table 3 Dye loading amounts and photovoltaic properties of the solar cells measured while ZnO were used as scatter layers under AM1.5G filtered 100 mW cm^2 illumination: short circuit current (J_{SC}), open circuit voltage (V_{OC}), fill factor (*FF*) and overall conversion efficiency (η)

sample	J_{SC}/ mA	V_{OC}/mV	*FF*/%	η/%
P25+sample **1**	13.46	0.76	65.88	6.74
P25+NP	12.47	0.76	64.47	6.11
P25	11.50	0.71	65.81	5.37

Conclusions

Glutamic acid was used as the configuration agent to synthesize ZnO nanoaggregates with different morphologies via the hydrothermal method. The ZnO nanoaggregates were first employed as photoanode materials in DSSCs. A *PCE* up to 4.52 % was achieved by using ZnO nanoaggregate featured with cauliflower-like microsphere structure, compared to a *PCE* of 3.73% obtained for a ZnO NP-based DSSC. Furthermore, when these ZnO nanoaggregates were used as scattering layers for P25-based DSSCs, the highest efficiency of 6.74% was achieved, compared with 5.37% obtained for single P25-based DSSC without any scattering layers, which indicates the conversion efficiency is increased by 25.5%.

Acknowledgements

This work is supported by National Natural Science Foundation of China (No. 21076147), Natural Science Foundation of

Tianjin (No.10JCZDJC23700) and China International Science and Technology Project (No. 2012DFG41980).

Notes and references

[a] School of Chemical Engineering and Technology, Tianjin University, Tianjin 300072, PR China
[b] Collaborative Innovation Center of Chemical Science and Engineering, Tianjin 300072, PR China
*Corresponding author. Tel./fax: +86 22 27892323.
**Corresponding author at: School of Chemical Engineering and Technology, Tianjin University, Tianjin 300072, PR China.
Tel./fax: +86 22 27892323.
E-mail addresses: baozhang@tju.edu.cn (B. Zhang), yqfeng@tju.edu.cn (Y. Feng).

† Electronic Supplementary Information (ESI) available: SEM images of the experiment of the formation of nanorods and the "time-dependent experiment". See DOI: 10.1039/b000000x/

1. B. O'Regan and M. Grätzel, *Nature*, 1991, 353, 737.
2. X. Peng, Y. Q. Feng and S. X. Meng, *Electrochimica Acta*, 2014, 115, 255.
3. Y. G. Tao, Y. Q. Xu and J. Pan, *Mat. Sci. Eng. B*, 177 (2012) 1664-1671.
4. M. K. Nazeeruddin, F. D. Angelis, S. Fantacci, A. Selloni, G. Viscardi, P. Liska, S. Ito, B. Takeru and M. Gra¨tzel, *J. Am. Chem. Soc.*, 2005, 127, 16835.
5. S. Mathew, A. Yella and P. Gao, *Nat. Chem.*, 2014, 6, 242.
6. Q. F. Zhang, T. P. Chou and B. Russo, *Angew. Chem. Int. Ed.*, 2008, 47, 2402.
7. M. Quintana, T. Edvinsson and A. Hagfeldt, *J. Phys. Chem. C*, 2007, 111, 1035.
8. R. Wahab, S. G. Ansari and Y. S. Kim, *Mater. Res. Bull.*, 2007, 42, 1640.
9. Q. Z. Wu, X. Chen and P. Zhang, *Cryst. Growth Des.*, 2008, 8, 3010.
10. Q. F. Zhang, C. S. Dandeneau and X. Y. Zhou, *Adv. Mater.*, 2009, 21, 4087.
11. T. M. ElAgez, A. A. El Tayyan and A. Al-Kahlout, *Inter. J. Mater. Chem*., 2012, 2, 105.
12. Q. Wan, Q. H. Li and Y. J. Chen, *Appl. Phys. Lett*., 2004, 84, 3653.
13. Y. P. Fang, Q. Pang and X. G. Wen, *Small*, 2006, 2, 612 – 615.
14. Y. J. Xing, Z. H. Xi and Z. Q. Xue, *Appl. Phys. Lett*., 2003, 83, 1689.
15. J. Zhang, W. Y. Yu and L. Zhang, *Phys. Lett. A*, 2002, 299, 276.
16. J. Q. Hu, Y. Bando and J. H. Zhan, *Appl. Phys. Lett*., 2003, 83, 24.
17. H. Kou, J. Wang and Y. B. Pan, *Mater. Chem. Phys*., 2006, 99, 325–328.
18. X. B. Lu, H. J. Zhang and Y. W. Ni, *Biosens. Bioelectron*., 2008, 24, 93.
19. J. M. Jang, C. R. Kim and H. Ryu, *J. Alloy. Compd.*, 2008, 463, 503.
20. Z. Fang, K. Tang and G. Z. Shen, *Mater. Lett*., 2006, 60, 2530.
21. Q. F. Zhang, T. P. Chou and B. Russo, *Angew. Chem. Int. Ed*., 2008, 120, 2436.
22. N. Memarian, I. Concina and A. Braga, *Angew. Chem. Int. Ed*., 2011, 123, 12529 .
23. X. H. Lu, Y. Z. Zheng and S. Q. Bi, *Adv. Energy Mater*., 2014, 130, 1802.
24. W. W. Sun, T. Peng and Y. M. Liu, *ACS Appl Mater Inter*, 2014, 6, 9144.
25. K. Mahmood and H. J. Sung, *J. Mater. Chem. A*, 2014, 2, 5408.
26. B. Weintraub, Z. Z. Zhou and Y. H. Li, *Nanoscale*, 2010, 2, 1573.
27. J. Liu, A. X. Wei, Y. Zhao, *J. Mater. Sci. Mater. Electron*, 2014, 25, 1122.
28. Y. M. Liu, H. W. Zhai and F. Guo, *Nanoscale*, 2012, 4, 6863–6869.